Article:
Fattah Poor, S, Hoang, TB, Midolo, L et al. (8 more authors) (2013) Efficient coupling of single photons to ridge-waveguide photonic integrated circuits. Applied Physics Letters, 102 (13). 131105. ISSN 0003-6951

https://doi.org/10.1063/1.4799669

Efficient coupling of single photons to ridge-waveguide photonic integrated circuits

S. Fattah poor,[1,a)] T. B. Hoang,[1] L. Midolo,[1] C. P. Dietrich,[1] L. H. Li,[2] E. H. Linfield,[2] J. F. P. Schouwenberg,[1] T. Xia,[1] F. M. Pagliano,[1] F. W. M. van Otten,[1] and A. Fiore[1]
[1]*COBRA Research Institute, Eindhoven University of Technology, P.O. Box 513, NL-5600MB Eindhoven, The Netherlands*
[2]*School of Electronic and Electrical Engineering, University of Leeds, Leeds LS2 9JT, United Kingdom*

(Received 15 February 2013; accepted 21 March 2013; published online 3 April 2013)

We demonstrate the efficient coupling of single photons emitted by single quantum dots (QDs) in a photonic crystal cavity (PhCC) to a ridge waveguide (RWG). Using a single-step lithographic process with an optimized tapering, up to 70% coupling efficiency between the photonic crystal waveguide and the RWG was achieved. The emission enhancement of single QDs inside an in-line PhCC coupled via the RWG to a single-mode fiber was observed. Single-photon funneling rates around 3.5 MHz from a single QD into the RWG were obtained. This result is a step toward the realization of a fully functional quantum photonic integrated circuit. © *2013 American Institute of Physics*. [http://dx.doi.org/10.1063/1.4799669]

Single photons are one of the most promising candidates for the implementation of quantum computation and quantum simulation, due to their low decoherence.[1–3] On-demand and on-chip generation and control of single photons are the main issues to be addressed for this purpose. Semiconductor quantum dots (QDs) have attracted considerable attention as single-photon sources because of their potential for integration with a semiconducting photonic integrated circuit.[4] The integration of QDs with photonic crystal (PhC) structures has been previously addressed and important functionalities such as efficient coupling of the emission of single QDs into photonic crystal cavities (PhCCs) and waveguides (PhCWGs) have been demonstrated.[5–12,16] Recently, approaches to reproducibly control the exciton and cavity energy on chip, as needed to realize a scalable circuit, have been developed.[13–15] However, quantum photonic integrated circuits cannot be practically implemented with these suspended structures due to their low mechanical stability and high optical loss. Although ridge waveguides (RWGs) are widely used for low-loss, on-chip transmission,[17] and their coupling with photonic nanostructures has been studied,[18–20] the efficient coupling of single photons from a single QD in a PhCC to a RWG has not been addressed. In this letter, we propose a design to overcome the mode mismatch between the RWG and the suspended PhC structure and demonstrate the efficiency of our method by transmission measurement and through the detection of single photons at the end of the RWG.

Our approach is shown in Figure 1(a) and consists of a first transition between the PhCWG and a suspended nanobeam (SNB), whose width is then adiabatically increased to the typical width ($3-5\,\mu$m) of a RWG. The PhCWG and the SNB are fabricated from a GaAs/AlGaAs heterostructure by reactive ion etching of the AlGaAs sacrificial layer. When the width of the SNB exceeds twice the lateral extent of AlGaAs etching, a supporting post is left and the structure evolves towards a conventional RWG (Ref. 18) (see the cross-sectional scanning-electron microscope (SEM) image in Figure 2(a)). In order to maximize the coupling efficiency between the PhCWG and the SNB (Ref. 21), the width of the SNB is chosen equal to $2a\sqrt{3}$ where a is the lattice constant of the PhC, five more holes are inserted in the SNB in continuation of the two inner hole rows of the PhCWG and their radii are tapered down in 10 nm steps (Figure 1(a)). According to simulations, this provides a 97% coupling efficiency between PhCWG and SNB.

We then calculated the coupling efficiency between SNB and RWG. Our RWG consists of a 4 μm wide and 320 nm thick slab of GaAs on top of a $Al_{0.7}Ga_{0.3}As$ sacrificial layer with 2.7 μm width and 1.5 μm thickness. The shape of the AlGaAs sacrificial layer in the simulation is considered according to the measured etching profile. We assume a SNB with 320 nm thickness and $2a\sqrt{3}$ width (with $a = 320$ nm). The fundamental transverse electric guided modes of the RWG and the SNB have been simulated (Figures 1(c) and 1(d)). A clear mode mismatch between the two modes is observed in both the lateral and vertical directions which would result in poor coupling efficiency if the two structures were coupled directly. Instead the tapering of the SNB width and of the supporting post ensures an adiabatic transition. Figure 1(b) illustrates the evolution of the transverse electric guided mode at the interface between the SNB and the RWG. The parameters considered here are the same as in Figures 1(c) and 1(d) except that the length of the taper and the initial width of the RWG are 10 μm and 3 μm, respectively, due to computational limitations. These calculations show that about 98% of the power is transmitted from the SNB to the RWG. We note that this tapered transition can be realized with a single step of lithography and etching, without the need for a critical realignment.

The fabrication was done on a sample grown by molecular beam epitaxy on an undoped GaAs substrate where a layer of GaAs with 320 nm thickness including low-density InAs QDs (Ref. 22) was grown on top of a 1.5 μm thick layer of $Al_{0.7}Ga_{0.3}As$. We begin by depositing a 400 nm thick layer of SiN as hard mask. A 320 nm thick layer of ZEP520A as electron beam resist is deposited in the next step. Our design

a)E-mail: s.fattahpoor@tue.nl

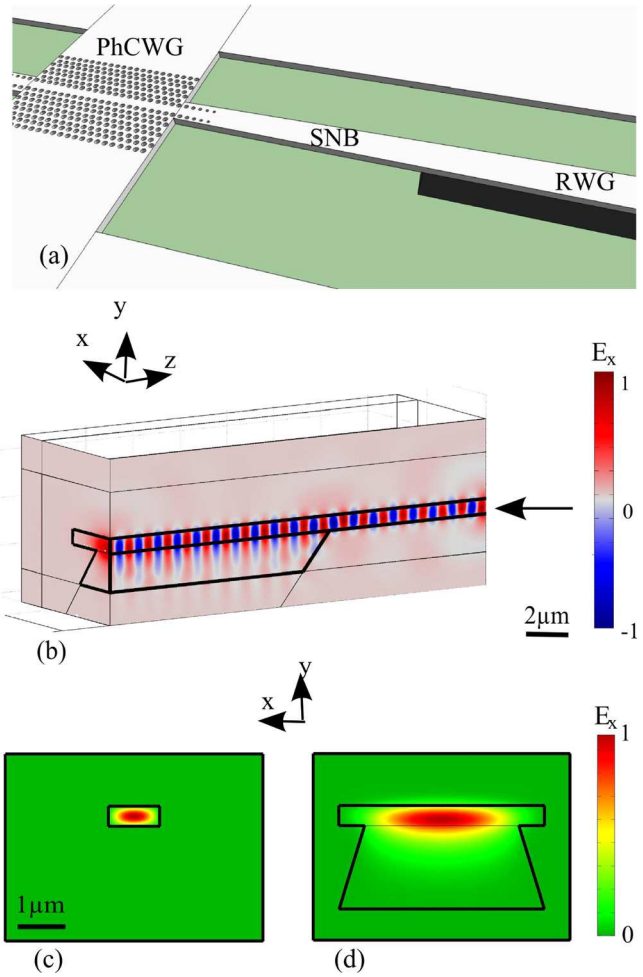

FIG. 1. (a) A sketch of the design where the interface between SNB, PhCWG, and RWG is shown. (b) Evolution of the normalized transverse-electric guided mode at the interface between SNB and RWG. The arrow indicates the input port used for calculation of the transmission in the structure. (c) and (d) Normalized transverse-electric guided mode profile at the entrance of the SNB and RWG, respectively.

including RWGs and PhC structures is exposed with 30 kV electron beam lithography and developed afterwards with n-amylacetate. Two subsequent dry etching steps (Reactive Ion Etching and Inductively Coupled Plasma etching) are performed in order to etch through the SiN and GaAs layers. The sacrificial layer is removed by wet etching in a HCl-based solution which results in a geometrically well defined etching profile due to different etching rates in different crystallographic orientations in AlGaAs (Figure 2(a)). The etching profile shown in Figure 2(a) is obtained when the RWGs are patterned and etched along the $[0\bar{1}1]$ crystallographic direction.[23] Finally, a dry etching with CF_4 is done to remove the SiN layer. The resulting devices are shown in Figures 2(a) and 2(b). In all the experiments described below, the initial width of the SNB is set to $2a\sqrt{3}$ and it is tapered to a RWG width of 4 μm at the cleaved facet.

To measure the coupling efficiencies in our system, we started by measuring the transmission through a simple RWG with 4 μm width and 1.6 mm length at room temperature. A tunable continuous wave laser is sent through an end-fire transmission measurement set-up which has two 50 × objectives (NA = 0.4) for side collection and excitation. The plot of the transmission as a function of the wavelength

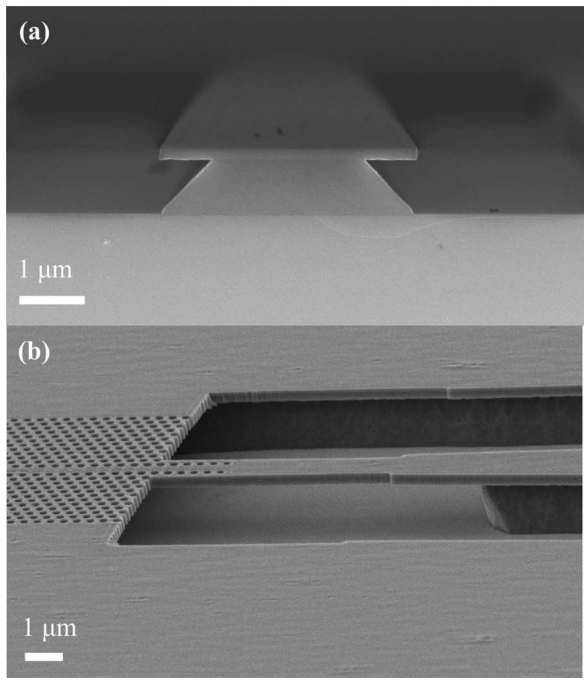

FIG. 2. SEM image of the fabricated devices at (a) entrance of a RWG with 4 μm width and (b) interface of the suspended and ridge structures.

for the RWG is shown in Figure 3(a) where the Fabry-Perot (FP) fringes due to the reflections at the two cleaved facets are evident. By fitting the transmission function for the RWG, we extract[24] the value of the loss per unit length $\alpha \approx 4 - 5\,\mathrm{cm}^{-1}$. This is a rather small loss considering the tight optical confinement in our RWG design. From the fit it is also possible to extract[24] the coupling efficiency (C_{RWG}) between the fiber and the center of the RWG, which for this measurement is $C_{RWG} = 3.78\%$. In the following, we use the spectrally averaged fiber-to-fiber transmission $\overline{T}_1$ (indicated by horizontal solid red line in Figure 3(a)) to give an approximate value of the coupling efficiency $\overline{C}_{RWG}$: $\overline{T}_1 \simeq \overline{C}^2_{RWG}$. The value of the transmission (fiber-in, fiber-out power ratio), averaged over the spectral region shown in Figure 3(a), was measured on four nominally identical RWGs, giving a value of $\overline{T}_1 = 0.138 \pm 0.005\%$ and $\overline{C}_{RWG} = 3.72 \pm 0.07\%$, which agrees well with the value obtained from the fitting.

The transmission through a symmetric RWG-PhCWG-RWG system was then measured. The PhCWG here is a triangular PhC with $L = 20\,\mu$m length (filling factor $FF = 31\%$, lattice constant a = 320 nm) and the two SNB-PhCWG transitions are tapered as described previously. The spectral transmission of the RWG-PhCWG-RWG system shown in the inset of Figure 3(b) over a large range, shows a clear signature of the dispersion edge of the even mode of the PhCWG around 1.32 μm. A high-resolution wavelength scan is shown in the main panel of the Figure 3(b) around 1.29 μm and in the high transmission spectral region of the PhCWG. Similar FP fringes were observed in four nominally identical waveguides. The system considered here can be described as a three-layer Fabry-Perot etalon with the corresponding multiple Fourier components which make a reliable fitting of the experimental data difficult, motivating our use of the spectrally integrated transmission. The average transmission in this spectral range was measured to

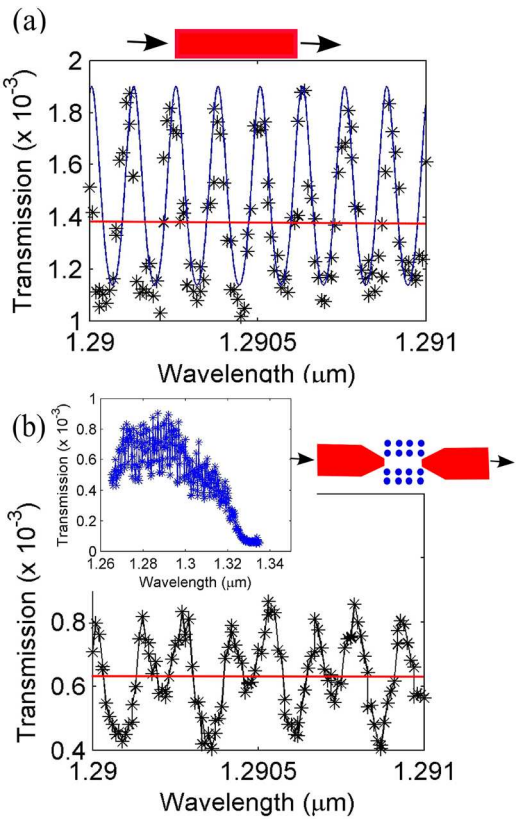

FIG. 3. Plot of the transmission versus wavelength for a (a) RWG (the blue and the red horizontal lines are the fit to the experimental data and the average transmission for the measured RWG, respectively). The inset illustrates a sketch of the system measured and (b) RWG-PhCWG-RWG system. The left inset shows the RWG-PhCWG-RWG transmission over a broader spectral range and the right inset illustrates a sketch of the system measured. The red horizontal line indicates the average transmission for the measured RWG-PhCWG-RWG system.

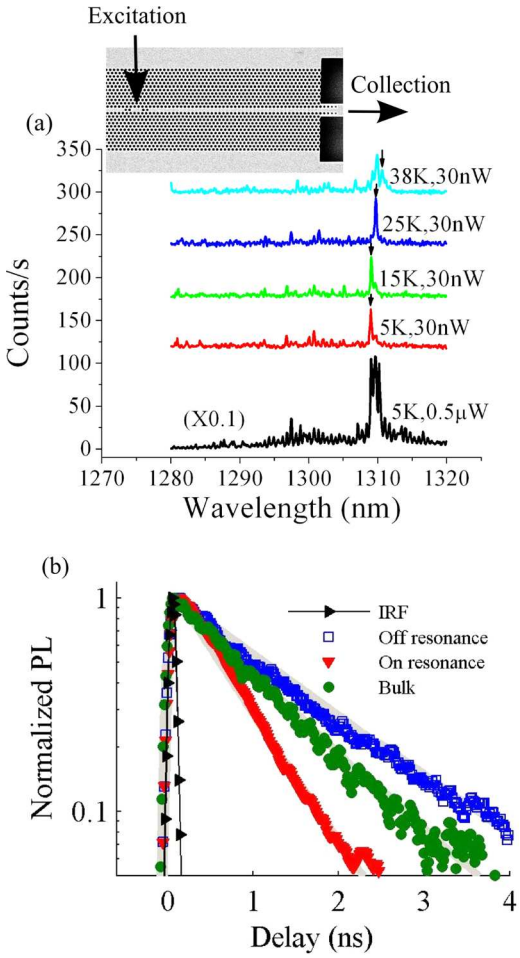

FIG. 4. (a) PL spectra of a QD in an L3 cavity coupled in-line to a PhCWG and then to a RWG, recorded at different temperatures. The curves are offset for clarity. The inset shows the SEM image of the PhCC (b) Time-resolved PL of the dot indicated by the arrow at 25 K (on-resonance, red triangles) and 38 K (off resonance, blue rectangles) collected from the side. The PL decay of a dot in the bulk (green circles, measured from the side) is shown for comparison. The decay curves have been normalized and the mono-exponential fits (grey lines) are obtained after convolution with the measured instrument response function (IRF) (black triangles).

be $\overline{T}_2 = 0.067 \pm 0.004\%$ on the four waveguides. Denoting the coupling efficiency at the interface between RWG and PhCWG as $\overline{C}_{PWG}$, we have: $\overline{T}_2 \simeq \overline{C}^2_{PWG} \times \overline{C}^2_{RWG}$. From the values of $\overline{T}_1$ and $\overline{T}_2$, we find $\overline{C}_{PWG} = 0.696 \pm 0.008$ meaning that ~70% of power from the PhCWG is coupled to the RWG. Also we conclude that a fraction $\overline{C}_{PWG} \times \overline{C}_{RWG} = 2.60 \pm 0.08\%$ of the power in the center of the PhCWG is coupled to the single mode fiber.

The final series of measurements is performed on a sample which is composed of a L3 cavity[25] coupled in-line to a PhCWG with two holes (the radius of the second hole is reduced by 10% with respect to the first one) as connecting barriers (see inset of Figure 4(a)). The PhCC-PhCWG system is subsequently coupled to the RWG with 400 μm length and 4 μm entrance width (lattice constant of PhC $a = 330$ nm). The sample is cooled down to 5 K in a different end-fire set-up with lensed-fibers (NA = 0.33) mounted on piezo-electric positioners for side collection and excitation and an objective (NA = 0.5) for top pumping. First a pulsed laser emitting at $\lambda = 757$ nm (repetition rate = 80 MHz, pulse width = 70 ps) is applied with 0.5 μW average power to the cavity from the top and the resulting photoluminescence (PL) coupled to the single-mode fiber via the RWG is collected from the side, dispersed by a $f = 1$ m spectrometer and detected by an InGaAs array detector. A peak at $\lambda = 1309.7$ nm (Figure 4(a)—black spectrum) is observed which corresponds to the cavity mode ($Q \simeq 1000$) and is pumped by the QD multiexcitonic background.[26,27] This peak is modulated by FP fringes due to reflections at the cleaved facet and at the interface between RWG and SNB ($L = 400\,\mu$m). By applying a pulsed quasi-resonant laser ($\lambda = 1064$ nm, repetition rate = 62 MHz, pulse width = 6 ps), the cavity mode was not observed anymore. Reducing the power to 30 nW resulted in the observation of single dot lines (colored spectra in Figure 4(a)). The temperature of the sample was increased from 5 K to 38 K and the spectral evolution of the single QD indicated by the arrow was recorded. The QD red-shifted by around 1.6 nm in this temperature range. The PL of the QD in and out of resonance with cavity mode (at 25 and 38 K) was filtered by a tunable filter and sent to a superconducting single photon detector (SSPD),[28] whose output was sent to a correlation card with 4 ps timing resolution. The obtained time-resolved PL spectra showed a change of the lifetime of the QD from $\tau = 0.67 \pm 0.02$ ns where it was in resonance with the cavity mode (25 K) to $\tau = 1.47 \pm 0.03$ ns for the situation where it was detuned 1.0 nm from the center of the cavity mode (38 K) (Figure 4(b)). This change of the spontaneous emission

rate is due to the change of the optical density of states and is here limited by the impossibility to tune the QD more than 1.0 nm away from the cavity wavelength. On QDs in the RWG but outside of the PhC region we measured a lifetime $\tau = 1.11 \pm 0.06$ ns (Figure 4(b)) while for the QDs in the PhC but out of resonance in similar PhC structures we previously measured decay times of 3-6 ns.[15] Based on this, we estimate a Purcell enhancement factor of $F_p \simeq 1.5$ and a coupling efficiency of $\beta \simeq 84\%$ of the QDs into the cavity mode.

Ultimately the non-classical (single-photon) nature of the emission from the single QDs into the RWG was investigated. The emission of the aforementioned dot at 25 K, under pumping with the pulsed quasi-resonant laser with the same power as in Figure 4, is coupled from the side by RWG to the single mode fiber and filtered by the tunable filter and consequently sent to a fiber-based Hanbury Brown-Twiss interferometer based on two SSPDs.[29] A clear dip can be observed at zero delay $\tau = 0$ ns in the corresponding coincidence rate (Figure 5) and from the ratio of the coincidence counts at zero delay (integrated over a 6 ns time window) to the average of the counts at the multiples of the repetition period, we estimate a $g^{(2)}(0) \simeq 0.42$. The discrepancy between the experimental value and the perfect single-photon case can be attributed to the residual background emission not completely filtered due to the limited bandwidth (0.8 nm) of our tunable filter.

To estimate the funnelling rate of single photons into the RWG (R_{RWG}), we measured the combined detection rate from both SSPDs during the anti-bunching measurement to be around 10 kHz. Taking into account the coupling efficiency from the center of the RWG to the single-mode fiber in the set-up with lensed-fibers, which was measured to be $C'_{RWG} = 7\%$, the transmission of our tunable filter which is equal to 40%, and the quantum efficiency of the SSPD $QE = 10\%$, we determine $R_{RWG} = 3.5$ MHz. When compared to the 62 MHz repetition rate of the laser, this indicates a probability of around 6% to produce a single photon in the RWG for each laser pulse. This value is partly limited by the coupling efficiency between PhCC and PhCWG, estimated as $\frac{1}{2} \times Q_{\text{loaded}} \times (Q^{-1}_{\text{loaded}} - Q^{-1}_{\text{unloaded}}) \simeq 0.2$, where Q_{loaded} and Q_{unloaded} are the quality factors of the PhCC with and without the PhCWG, respectively, as measured on a similar PhCC. An additional limitation is given by the competing emission channels from charged and multi-exciton states in the QD, which prevent reaching the saturated emission rate. The PhC coupling efficiency can be improved by optimized design and fabrication, while the QD charge state may be controlled by the application of an electric field,[26] which would also be beneficial for controlling the QD-PhCC spectral coupling.[15]

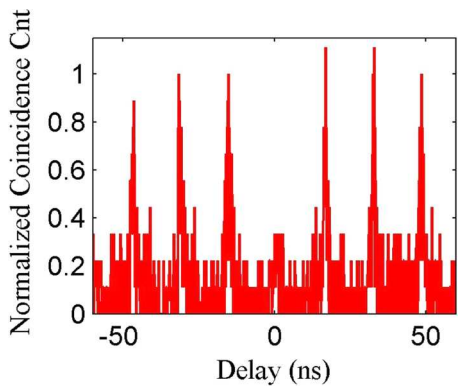

FIG. 5. Normalized coincidence counts of the QD indicated by arrow in Figure 4 at 25 K coupled from the side to a Hanbury Brown-Twiss set-up.

In summary, a design has been proposed for the efficient coupling between a PhC structure and a RWG. The devices fabricated with this design have shown a high value of around 70% for the coupling efficiency between PhCWG and RWG. The emission of single QDs coupled to the RWG has been collected from the side and its rate enhancement with tuning in and out of resonance has been observed. The single photon nature of the detected emission has also been proven. These results represent a step towards the realization of a fully functional quantum photonic integrated circuit, including single photon detectors.[30]

We thank S. Assali for technical assistance. Financial support by the TU/e High Potential program, EU-FP7 QUANTIP project (Project No. 244026) and the Dutch Technology Foundation STW (Project No. 10380) is acknowledged. The nanofabrication was carried out in the NanoLab@TU/e cleanroom facility.

[1]J. L. O'Brien, Science **318**, 1567 (2007).
[2]E. Knill, R. Laflamme, and G. J. Milburn, Nature **409**, 46 (2001).
[3]L. M. Duan and H. J. Kimble, Phys. Rev. Lett. **92**, 127902 (2004).
[4]A. J. Shields, Nature Photon. **1**, 215 (2007).
[5]A. Badolato, K. Hennessy, M. Atature, J. Dreiser, P. M. Petroff, and A. Imamoglu, Science **308**, 1158 (2005).
[6]D. Englund, D. Fattal, E. Waks, G. Solomon, B. Zhang, T. Nakaoka, Y. Arakawa, Y. Yamamoto, and J. Vuckovic, Phys. Rev. Lett. **95**, 013904 (2005).
[7]L. Balet, M. Francardi, A. Gerardino, N. Chauvin, B. Alloing, C. Zinoni, C. Monat, L. H. Li, N. Le Thomas, R. Houdre, and A. Fiore, Appl. Phys. Lett. **91**, 123115 (2007).
[8]V. S. Rao and S. Hughes, Phys. Rev. Lett. **99**, 193901 (2007).
[9]T. Lund-Hansen, S. Stobbe, B. Julsgaard, H. Thyrrestrup, T. Sunner, M. Kamp, A. Forchel, and P. Lodahl, Phys. Rev. Lett. **101**, 113903 (2008).
[10]T. B. Hoang, J. Beetz, L. Midolo, M. Skacel, M. Lermer, M. Kamp, S. Höfling, L. Balet, N. Chauvin, and A. Fiore, Appl. Phys. Lett. **100**, 061122 (2012).
[11]A. Enderlin, Y. Ota, R. Ohta, N. Kumagi, S. Ishida, S. Iwamoto, and Y. Arakawa, Phys. Rev. B **86**, 075314 (2012).
[12]A. Laucht, S. Pütz, T. Günther, N. Hauke, R. Saive, S. Frederik, M. Bichler, M. C. Amann, A. W. Holleitner, M. Kaniber, and J. J. Finley, Phys. Rev. X **2**, 011014 (2012).
[13]R. B. Patel, A. J. Bennett, I. Farrer, C. A. Nicoll, and A. J. Shields, Nature Photon. **4**, 632 (2010).
[14]L. Midolo, F. Pagliano, T. B. Hoang, T. Xia, F. W. M. van Otten, L. H. Li, E. H. Linfield, M. Lermer, S. Höfling, and A. Fiore, Appl. Phys. Lett. **101**, 091106 (2012).
[15]T. B. Hoang, J. Beetz, M. Lermer, L. Midolo, M. Kamp, S. Höfling, and A. Fiore, Opt. Express **20**, 21758 (2012).
[16]A. Schwagmann, S. Kalliakos, J. D. P. Ellis, I. Farrer, J. P. Griffiths, G. A. C. Jones, D. A. Ritchie, and A. J. Shields, Opt. Express **20**, 28614 (2012).
[17]I. Hiroaki, K. Hiruma, K. Ishida, T. Asai, and H. Matsumura, IEEE Trans. Electron Devices **32**, 2662 (1985).
[18]C. Baker, C. Belacel, A. Andronico, P. Snellart, A. Lemaitre, E. Galopin, S. Ducci, G. Leo, and I. Favero, Appl. Phys. Lett. **99**, 15117 (2011).
[19]A. Talneau, K. H. Lee, S. Guilet, and I. Sagnes, Appl. Phys. Lett. **92**, 061105 (2008).
[20]M. G. Banaee, A. G. Pattantyus-Abraham, M. W. McCutcheon, G. W. Rieger, and J. Y. Young, Appl. Phys. Lett. **90**, 193106 (2007).
[21]L. Rosa, S. Selleri, and F. Poli, J. Lightwave Technol. **23**, 2740 (2005).

[22]L. H. Li, N. Chauvin, G. Patriarche, B. Alloing, and A. Fiore, J. Appl. Phys. **104**, 083508 (2008).
[23]R. P. Ribas, J. L. Leclercq, J. M. Karam, B. Courtois, and P. Viktorovitch, Mater. Sci. Eng., B **51**, 267 (1998).
[24]A. De Rossi, V. Ortiz, M. Calligaro, L. Lanco, S. Ducci, V. Berger, and I. Sagnes, J. Appl. Phys. **97**, 073105 (2005).
[25]A. R. A. Chalcraft, S. Lam, D. O'Brien, T. F. Krauss, M. Sahin, D. Szymanski, D. Sanvitto, R. Oulton, M. S. Skolnick, M. A. Fox, D. M. Whittaker, H. Y. Liu, and M. Hopkinson, Appl. Phys. Lett. **90**, 241117 (2007).
[26]N. Chauvin, C. Zinoni, M. Francardi, A. Gerardino, L. Balet, B. Alloing, L. H. Li, and A. Fiore, Phys. Rev. B **80**, 241306(R) (2009).
[27]M. Winger, T. Volz, G. Tarel, S. Portolan, A. Badolato, K. J. Hennessy, E. L. Hu, A. Beveratos, J. J. Finley, V. Savona, and A. Imamoglu, Phys. Rev. Lett. **103**, 207403 (2009).
[28]G. N. Gol'tsman, O. Okunev, G. Chalkove, A. Lipatov, A. Semenov, K. Smirnov, B. Voronov, A. Dzardanov, C. Williams, and R. Sobolevski, Appl. Phys. Lett. **79**, 705 (2001).
[29]C. Zinoni, B. Alloing, C. Monat, V. Zwiller, L. H. Li, A. Fiore, L. Lunghi, A. Gerardino, H. de Riedmatten, H. Zbinden, and N. Gisin, Appl. Phys. Lett. **88**, 131102 (2006).
[30]J. P. Sprengers, A. Gaggero, D. Sahin, S. Jahanmirinejad, G. Frucci, F. Mattioli, R. Leoni, J. Beetz, M. Lermer, M. Kamp, S. Höfling, S. Sanjines, and A. Fiore, Appl. Phys. Lett. **99**, 181110 (2011).